Curvature, metric and parametrization of origami tessellations: Theory and application to the eggbox pattern

H. Nassar[a,b], A. Lebée[a,*], L. Monasse[b]

[a] *Laboratoire Navier, Ecole des Ponts-ParisTech, IFSTTAR, CNRS, UPE, 6 et 8 Avenue Blaise Pascal, 77455 Marne-la-Vallée cedex 2*
[b] *Université Paris-Est, Cermics (ENPC), INRIA, F-77455 Marne-la-Vallée*

Abstract

Origami tessellations are particular textured morphing shell structures. Their unique folding and unfolding mechanisms on a local scale aggregate and bring on large changes in shape, curvature and elongation on a global scale. The existence of these global deformation modes allows for origami tessellations to fit non-trivial surfaces thus inspiring applications across a wide range of domains including structural engineering, architectural design and aerospace engineering. The present paper suggests a homogenization-type two-scale asymptotic method which, combined with standard tools from differential geometry of surfaces, yields a macroscopic continuous characterization of the global deformation modes of origami tessellations and other similar periodic pin-jointed trusses. The outcome of the method is a set of non-linear differential equations governing the parametrization, metric and curvature of surfaces that the initially discrete structure can fit. The theory is presented through a case study of a fairly generic example: the eggbox pattern. The proposed continuous model predicts correctly the existence of various fittings that are subsequently constructed and illustrated.

Keywords: Origami, Metasurface, Form finding, Floppy modes, Eggbox

*Corresponding author (arthur.lebee@enpc.fr)

1. Introduction

Origami based materials have proven to be useful in various domains ranging from structural engineering, to architectural design and aerospace engineering (Hochfeld, 1959; Lebée, 2015; Miura, 1985; Peraza-Hernandez et al., 2014; Resch and Christiansen, 1970). Today, origami keeps inspiring a class of novel structures exhibiting interesting non-standard properties gathered under the name of metamaterials or metasurfaces (Lv et al., 2014; Schenk and Guest, 2013; Silverberg et al., 2014; You, 2014). There is therefore, in parallel with a rapidly expanding array of applications, a growing need for mechanical modelling tools well adapted to origami-folded structures.

An origami-folded structure often presents as a polyhedral surface where planar facets intersect along straight edges marking creases. When the structure moves and deforms, creases behave like hinges opening and closing folds while facets stretch, twist and bend. These mechanisms compete energetically. Some of them are energetically costly and are blocked whereas others are activated and guide the global deformation of the structure. Often however, facets remain rigid (Lechenault et al., 2014) or at least rigid by parts (Demaine et al., 2011; Korte et al., 2010; Schenk and Guest, 2013). This means that when a facet deforms, new sub-creases emerge. Therefore, upon changing the crease pattern, it can be assumed that the dominant deformation modes of an origami-folded structure do not strain facets. These deformation modes are referred to as rigid foldings (Belcastro and Hull, 2002; Tachi, 2009). Given their low potential energy, rigid foldings can also be called compliant, floppy or even zero-energy deformation modes.

Texturing an initially flat sheet with a fine crease pattern has accordingly a great impact on the behaviour of the considered sheet. In fact, it predestines the sheet to deform conforming to one of its floppy modes into a three-dimensional shell structure bringing on large changes in curvatures and elongations. Furthermore, being bound by the rules of rigid folding, the set of independent degrees of freedom of the sheet is highly reduced. A crease pattern can then transform a flat sheet into a controllable deployable morphing shell structure with interesting applications in the field of form-finding.

Some rational approaches to origami-based form-finding, i.e., constructing specific three-dimensional shapes out of two-dimensional flat surfaces through folding, can be found in the book by Lang (2003). Later, Tachi (2010) suggested a more systematic method to "origamize" complex polyhedral surfaces. The method produces intricate crease patterns which fold into

desired shapes. The folding motion of these patterns seems however to be of a local nature: it only involves a few degrees of freedom at a time. In fact, crease patterns with mostly global deformation modes are more suited to the design of morphing shell structures. In this spirit, Tachi (2013), Zhou et al. (2015) and Dudte et al. (2016) provided new procedures that allow to, within a global deformation, rigidly fold a sheet into a target surface using variations of Miura's and Resch's crease patterns. Note that these patterns, in contrast to the ones by Tachi (2010), are uniform somehow since they have the same topology everywhere. Note also that they are not periodic because creases have lengths that vary in space.

When the crease pattern is periodic, one speaks of origami tessellations. Origami tessellations would be simpler to manufacture. Nonetheless, characterizing their motion remains a non-trivial task. For instance, Blinn (1988) relates how Resch's tessellation failed to fit an egg shape. He then goes on to formulate a set of open questions one of which is the center of our attention here: how to characterize the surfaces that can be fitted by a given origami tessellation.

In the present paper, inspired by homogenization theory, we suggest a homogenization-type two-scale asymptotic method which, combined with standard tools from differential geometry of surfaces, yields a continuous homogeneous description of the possible rigid foldings of origami tessellations. This entails that the large number of discrete equations coding the rules of rigid folding for each vertex, edge and facet can be condensed and upscaled into a few differential equations governing the parametrization, metric and curvature of surfaces that the tessellation can fit. The method is also applicable for a wider family of structures known as pin-jointed trusses, i.e., assemblies of rigid bars and pivots (Figures 1 and 2).

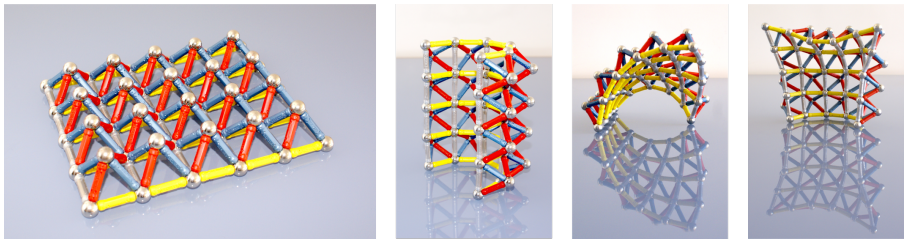

Figure 1. A pyramidal truss built with the magnetic construction set Geomag®. The involved mechanisms are the same as for rigid folding.

Characterizing the floppy modes of a structure further has its importance independently of the context of origami-folded structures. A structure having floppy modes usually means that its behaviour falls beyond classical elasticity and its modelling requires more exotic models. See for instance the pantographic structures considered by Seppecher et al. (2011) and by Dell'Isola et al. (2016). Other examples include pentamode materials, introduced by Milton and Cherkaev (1995) as materials with 5 floppy modes, and used by Norris (2008) to conceive acoustic invisibility cloaks.

More generally, upscaling discrete periodic structures into continuous homogeneous media is a recurrent topic in homogenization theory. The present approach features nevertheless a two-fold novelty. First, it is a purely geometric approach. As argued above, dismissing elastic effects is well-justified and suitable to describe the dominant deformation modes of an origami tessellation. Second, it accounts for large changes in metric and curvature commonly occurring during folding and unfolding motions.

The first significant step toward a continuous formulation of the fitting problem was made by Schenk and Guest (2013) and Wei et al. (2013). Building on the work of Norman (2009), Schenk and Guest (2011) and Seffen (2012), they calculated the in-plane and out-of-plane Poisson's ratios of the Miura-ori tessellation. Poisson's ratios carry local information on the coupling between elongations and curvatures in different directions. Here, once local characterizations are obtained through a two-scale asymptotic procedure, we go one step further and write global compatibility conditions in the form of three partial differential equations known as the Gauss-Codazzi-Mainardi equations (Ciarlet, 2006).

The rest of the paper goes as follows. In Section 2, the floppy modes of a periodic pyramidal truss are explored. A careful yet elementary analysis of the involved folding kinematics shows that it can only deform into developable surfaces to leading order. Section 3 then deals with the eggbox pattern. Though it cannot be rigidly folded from a flat sheet, the eggbox is still governed by the same rigid folding motion of a proper origami tessellation. Once introduced and parametrized, the deformation modes of the eggbox are scaled and asymptotically expanded in the limit where the unit-cell characteristic length r becomes close to 0. Consequently, the leading order term of the expansion describes the smooth surfaces $\mathscr{S}$ that the eggbox can deform into and fit asymptotically when r is much smaller than the radii of curvature of $\mathscr{S}$. Subsequently, surfaces $\mathscr{S}$ are characterized locally by two Poisson's ratios which, surprisingly, turn out to be equal and opposite, and

also equal and opposite to those of the Miura-ori tessellation. Finally, surfaces $\mathscr{S}$ are characterized globally as solutions to the Gauss-Codazzi-Mainardi equations. In Section 4, these equations are integrated under simplifying hypotheses such as axisymmetry. A rich family of solution surfaces $\mathscr{S}$ are then constructed and depicted as well as their fittings.

2. A pyramidal truss

Any smooth enough surface can be locally meshed with quadrilaterals by considering, for instance, the contour lines of any local coordinate system. Better yet, it is known that the quadrilaterals can be chosen to be rhombi of different interior angles. The resulting mesh is called a Chebyshev net (see, e.g., Ghys, 2011; Masson and Monasse, 2016; Samelson and Dayawansa, 2012). The pyramidal truss we examine next is a constrained Chebyshev net where all rhombi are required to belong to spheres of the same radius (Figure 2). We shall identify the smooth surfaces that this truss is able to fit when the size of the pyramids becomes infinitely small. In other, more mechanical, terms, we will describe the finitely deformed states that can be achieved by moving the assembly of rigid bars and pivots which is depicted in a reference plane configuration in Figure 2. Fairly simple arguments will lead to an equally simple solution and pave the way toward the more involved considerations of the next section.

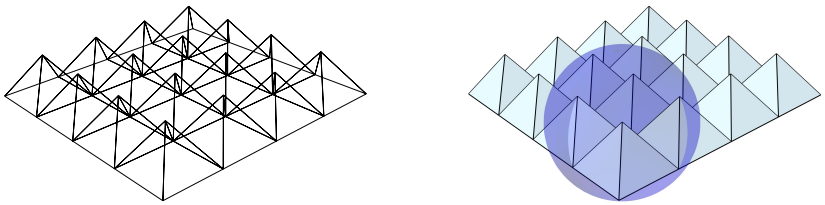

Figure 2. The pyramidal truss seen as made, to the left, of rigid bars (the edges) and pivots (the vertices) or, to the right, of an inextensible, paper-like, material that can only deform by folding along predefined crease lines (the edges). For all pyramids, the summit is constantly at the centre of a sphere of radius r containing the 4 vertices of the basis.

2.1. The kinematics of a single pyramid

Each pyramid of the pyramidal truss under consideration has a unique deformation mode which can be parametrized by the interior angle of its

basis: θ (see Figure 3). Indeed, knowing the positions of vertices A, B and D, vertex E is uniquely positioned at the intersection of three spheres centred at A, B and D and of the same radius r. Having E, C is similarly obtained. It

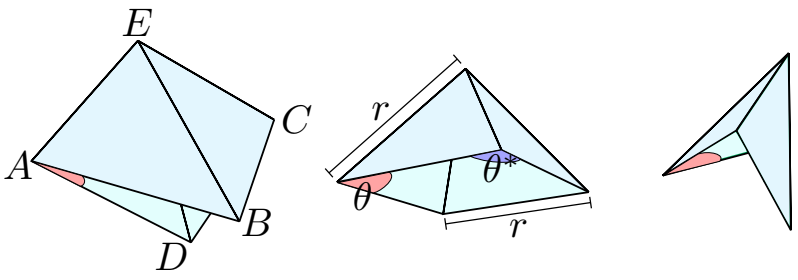

Figure 3. The deformation mode of a pyramid. Angle θ is comprised between 0 and $2\pi/3$.

is elementary to check that the angles $\widehat{DAB}$, $\widehat{DEB}$ and $\widehat{DCB}$ are identical and equal to θ. The "dual" three angles $\widehat{ABC}$, $\widehat{AEC}$ and $\widehat{ADC}$ are also identical and their value is called θ^* hereafter. With a small extra effort, we see that triangles AEC and DEB are in orthogonal planes and have a common altitude passing through E so that on the one hand

$$\left\langle \overrightarrow{AE}, \overrightarrow{BE} \right\rangle = r^2 \cos(\widehat{AEC}/2) \cos(\widehat{DEB}/2) = r^2 \cos(\theta^*/2) \cos(\theta/2)$$

holds and on the other hand

$$\left\langle \overrightarrow{AE}, \overrightarrow{BE} \right\rangle = r^2 \cos(\pi/3) = r^2/2$$

holds as well. In conclusion, θ and its dual are related through

$$2 \cos(\theta/2) \cos(\theta^*/2) = 1. \tag{1}$$

2.2. The kinematics of a single row

Stepping up, consider one fibre of the truss, i.e., a straight line of the reference configuration entirely composed of rigid bars, and assume its position to be known in the deformed configuration. Then, positioning any pyramid adjacent to that fibre is enough to uniquely position all adjacent pyramids of the same side by iterating the construction by intersecting spheres described

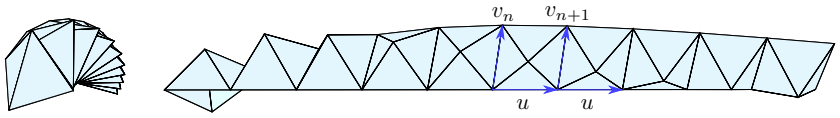

Figure 4. The propagation of a transverse vector along a rectilinear fibre; side view (left) and top view (right).

in the foregoing section. Figure 4 depicts the situation when the fibre remains rectilinear of constant direction u in the deformed state: given a transverse vector v_n, vector v_{n+1} can be uniquely determined.

The propagation of vector v_n in the direction of u appears to be composed of two parts: a shearing motion and a torsion motion around u. Quantitatively, letting θ_n be the angle between u and v_n, one has

$$\theta_{n+1} = \pi - \theta_n^*,$$

and, by virtue of Equation (1),

$$2\sin(\theta_{n+1}/2)\cos(\theta_n/2) = 1.$$

A quick trigonometrical manipulation eliminates recursion and implies that

$$\cos\theta_n = \frac{\cos\theta_0}{1 + n\cos\theta_0},$$

which is enough to determine θ_n since it is comprised between 0 and $2\pi/3$.

For increasing n, sequences (θ_n) exhibit different behaviours depending on whether some initial angle, denoted θ_0 above, is acute or obtuse.

1. $\theta_0 = \pi/2$ leaves the row of pyramids in its reference state and all subsequent angles are equally right.
2. $\theta_0 < \pi/2$ initiates an increasing sequence converging to $\pi/2$.
3. $\theta_0 > \pi/2$ initiates an increasing sequence which sooner or later surpasses $2\pi/3$. In this case, only a finite number of adjacent pyramids can be constructed in the direction of increasing n.

What is nonetheless surprising at first sight is that the above behaviour is scale- or r-invariant. Insisting further, let us call N the maximum number

of pyramids which can be constructed before the singularity predicted for an obtuse θ_0 manifests itself. Thus, the distance between pyramid number 0 and pyramid number N is Nr. For infinitely small r, the singularity becomes infinitely close to pyramid number 0 and forbids the construction of pyramids over any finite distance. For an acute θ_0, a discontinuous jump in θ from θ_0 to $\pi/2$ appears over an infinitely small distance.

In conclusion, it is impossible to define a continuous counterpart to the discrete sequence (θ_n), say $\theta(x)$ where x is the coordinate along the fibre, when r becomes infinitely small unless θ_0 was equal to $\pi/2$ or approached $\pi/2$ as r approached 0 in order to "push away" jumps and singularities.

2.3. Fitting a surface

When the vertices of a fibre describe a smooth non-rectilinear curve of curvature κ, our previous analysis holds locally over neighbourhoods of size R much smaller than the radius of curvature $1/\kappa$ and as long as r is sufficiently small compared to R, i.e., when

$$r \ll R \ll 1/\kappa. \tag{2}$$

This is due to the fact that smooth curves are locally straight. In any case then, a smooth counterpart to θ is either everywhere equal to $\pi/2$, to leading order in r, or is non-existent.

As for smooth surfaces $\mathscr{S}$ fitted by the pyramidal truss for infinitely small r, they host truss fibres as smooth paths. The preceding argument therefore entails that θ needs to be, exactly or asymptotically, equal to $\pi/2$ everywhere for the limit fitted surface to exist and be smooth. A direct consequence is that the fibres of the truss experience no shearing during the motion transforming the reference plane state into $\mathscr{S}$, to leading order in r. Being inextensible, they do not stretch either. Hence, the metric tensor of $\mathscr{S}$ is equal to that of a plane and $\mathscr{S}$ is necessarily a *developable* surface, i.e., of vanishing Gaussian curvature.

On Figure 1, the rightmost configuration exhibits some saddle-shaped points of negative Gaussian curvature. Note however that they only extend over a limited number of pyramids. Therefore, condition (2) is not satisfied and the above result is not contradicted. When trying to add more pyramids, one could feel the structure stiffening and some pyramids end up collapsing revealing geometrical incompatibilities.

Figure 5 portrays a fitted cone. The transformation being isometric, the straight lines of the reference state, such as the truss fibres, are mapped into

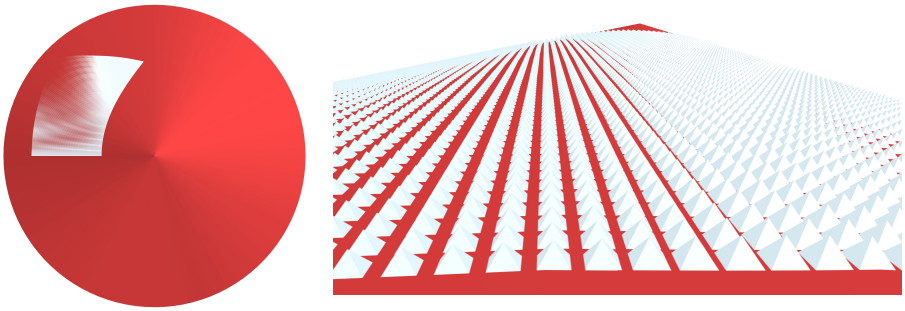

Figure 5. Fitting a cone. The fitted surface is of unitary area and r is of order $1/60$ in arbitrary units. At the top of the surface, the cone is of height $1/2$ and of radius $1/2$. The height of the pyramids can be interpreted as an error bar and shows that the fitting error is of order r.

cone geodesics. This observation provides a way to construct the pyramidal truss fitting a developable surface in three steps:

1. Choose two orthogonal geodesics of the developable surface and discretize them with a step equal to r.
2. By iterating the procedure described in the past section, propagate one geodesic along the other and obtain a discrete trussed surface.
3. Make r go to 0.

Last, note that due to Gauss's theorema egregium, Gaussian curvature only arises in surfaces of varying metric. Hence, fitting such surfaces should not be possible to leading order in r except with trusses which can accommodate the in-plane strains necessary for changing the metric. One such instance is the eggbox we study next.

3. The eggbox pattern

The eggbox is a pyramidal truss where the orientation of the pyramids alternates in a chequerboard-like fashion (Figure 6). After parametrizing and scaling its transformations, some asymptotic expansions will provide information on the metric and curvatures of the smooth surfaces $\mathscr{S}$ it can fit. In particular, it turns out that the in-plane and out-of-plane Poisson's ratios are equal and of opposite signs. Finally, a continuous formulation of the problem of fitting a surface $\mathscr{S}$ with an eggbox is given.

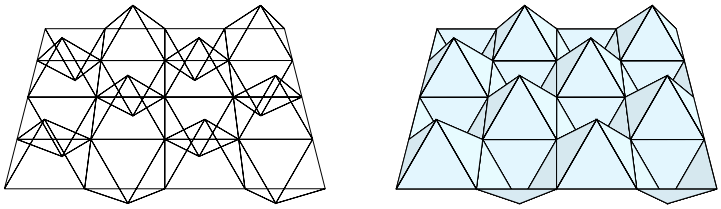

Figure 6. The eggbox in its reference state.

3.1. Preliminaries

The purpose of this section is to describe a particular parametrization of the eggbox and to introduce the useful notion of "equivalent vertices". Then, in the next section, we formulate the fitting problem and suggest a way to tackle it.

We have seen that the transformation of the pyramidal truss of Section 2 can be controlled through the transformation of a boundary composed of any couple of initially orthogonal fibres. Unsurprisingly, the same construction holds for the eggbox as long as we carefully alternate the pyramids orientation. However, considering our purpose, it is convenient to describe another way of controlling the transformation of the eggbox based on a couple of consecutive diagonals.

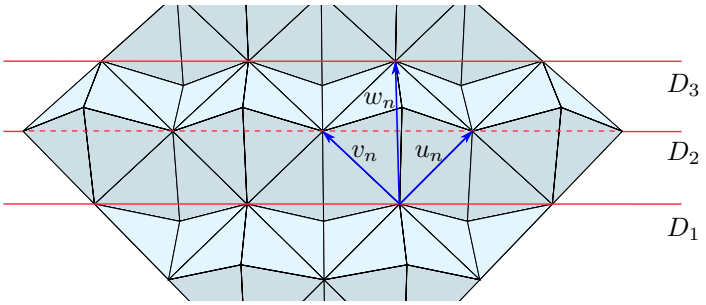

Figure 7. "Propagating" a diagonal: having u_n and v_n, vector w_n can be constructed. Therefore, having (D_1) and (D_2), diagonal (D_3) can be constructed.

As a matter of fact, from Figure 7, it is clear that knowing the positions of all the nodes located on two consecutive diagonals (D_1) and (D_2) is enough to uniquely position the nodes of the next diagonal (D_3). By constructing one diagonal after another, the whole eggbox can be controlled. Accordingly, it is possible to parametrize any configuration of the eggbox with two sequences of

unitary vectors joining the vertices of (D_1) and (D_2): $U = (u_n)$ and $V = (v_n)$, $n \in \mathbb{Z}$.

On a different note, the reference state depicted in Figure 6 will be qualified as *periodic* since it translates into itself by at least two independent vectors. In other words, there exists a unit-cell that can be translated around to tile the entire reference state with no gaps and no overlaps. When the tiling is carried out, one can deduce from each vertex M a set of *equivalent vertices* which are indistinguishable from M if not by their absolute position. These form a sequence with two-indices denoted as $(M_{i,j})$ and illustrated on Figure 8. Note that while the vertices of the eggbox in a periodic state do not all belong to the same plane, each set of equivalent vertices is planar.

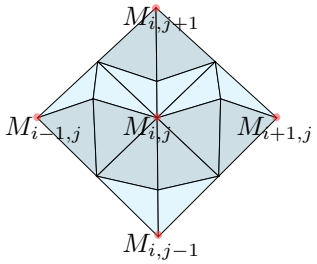

Figure 8. A set of indexed equivalent vertices.

3.2. The fitting problem

When the eggbox deforms, a set of equivalent vertices leaves its planar periodic reference state and maps some discrete surface S. Solving the fitting problem amounts to characterizing all possible surfaces S. Here, our purpose is to characterize the smooth surfaces $\mathscr{S}$ that S will fit when the side length of the pyramids r becomes infinitely small and to leading order in r.

Hence, let $\mathscr{S}$ be one such smooth surface and M be a point of $\mathscr{S}$. In order to fit $\mathscr{S}$, we start by considering an eggbox, or a portion thereof, and we deform it so that it fits a small neighbourhood of $\mathscr{S}$ containing M. We use one eggbox per point M. Each eggbox used is indexed with its corresponding point M and said to be "attached" to M. Last, we check if the different eggboxes can be made compatible, i.e., whether they merge into one single eggbox fitting $\mathscr{S}$ entirely.

Going further into details, by translating the eggbox attached to M, it is possible to ensure that M coincides with one of its vertices. Then, call

$$S(M) = \{M_{i,j}(U(M), V(M)), (i,j) \in \mathbb{Z}^2\}$$

the set of vertices equivalent to M in the eggbox attached to M. Therein,

$$U(M) = (u_n(M)) \quad \text{and} \quad V(M) = (v_n(M))$$

are the two sequences of unitary vectors controlling the eggbox attached to M. Upon translating both $\mathscr{S}$ and the eggbox, we may assume that M is placed at the origin $(0,0,0)$ of $\mathbb{R}^3$. Finally, let

$$rS^r(M) = \{rM_{i,j}(U^r(M), V^r(M)), (i,j) \in \mathbb{Z}^2\}$$

be the scaled set of equivalent vertices where the previously defined quantities now may vary when r goes to 0. For each scaling factor r, one tries to position the two sequences $U^r(M)$ and $V^r(M)$ in such a way that the vertices of $rS^r(M)$ best fits $\mathscr{S}$ over a small neighbourhood of M. By using an eggbox to fit $\mathscr{S}$ in the vicinity of each of its points and then "glueing" these eggboxes together, we fit $\mathscr{S}$ entirely.

The above procedure is reminiscent of the two-scale asymptotic expansions commonly used in homogenization of periodic structures. Here, point M is seen as a macroscopic point, i.e., the slow variable, whereas couples (i,j) indexing vertices of the attached eggbox are seen as microscopic or fast variables. In this comparison, fitting $\mathscr{S}$ locally corresponds to solving a unit-cell problem, one for each macroscopic point M, and fitting $\mathscr{S}$ globally corresponds to solving the global elastostatic boundary value problem.

Summing up, we proceed in two steps. First, necessary local compatibility conditions stating that it is possible to fit $\mathscr{S}$ in the vicinity of each of its points are obtained in the form of equations satisfied by the metric and curvatures of $\mathscr{S}$. Then, whether these metric and curvatures can be integrated, i.e., can be derived from a smooth parametrization of $\mathscr{S}$, is subject to some global compatibility conditions known as the Gauss-Codazzi-Mainardi equations.

3.3. Local compatibility conditions: on the metric

When r goes to 0, all vertices $rM_{i,j}(U^r(M), V^r(M))$ converge towards the origin of $\mathbb{R}^3$ where M is. Furthermore, we require that the finite differences of rank 1 converge toward their continuous counterparts which are

tangent vectors to $\mathscr{S}$ at M. Namely, we assume that there exists a smooth parametrization ϕ of two continuous variables x and y of $\mathscr{S}$ such that for all $(i,j) \in \mathbb{Z}^2$,

$$\frac{rM_{i+1,j}(U^r(M),V^r(M)) - rM_{i,j}(U^r(M),V^r(M))}{r} \xrightarrow[r\to 0]{} \partial_x\phi(x,y) \equiv \phi_x(x,y),$$
$$\frac{rM_{i,j+1}(U^r(M),V^r(M)) - rM_{i,j}(U^r(M),V^r(M))}{r} \xrightarrow[r\to 0]{} \partial_y\phi(x,y) \equiv \phi_y(x,y),$$

where (x,y) are the coordinates of M in the parametrization ϕ. Hence, for all $(i,j) \in \mathbb{Z}^2$,

$$M_{i+1,j}(U^0(M),V^0(M)) - M_{i,j}(U^0(M),V^0(M)) = \phi_x(x,y),$$
$$M_{i,j+1}(U^0(M),V^0(M)) - M_{i,j}(U^0(M),V^0(M)) = \phi_y(x,y).$$

As a result, $S^0(M)$ is a periodic plane configuration containing both $\phi_x(x,y)$ and $\phi_y(x,y)$: $S^0(M)$ fits the tangent plane of $\mathscr{S}$ at M (Figure 9).

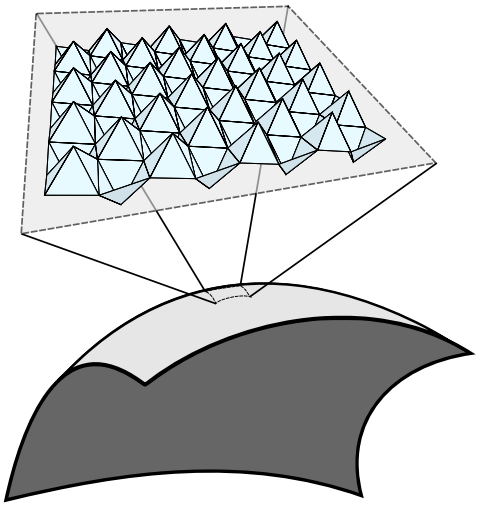

Figure 9. The blow up of an eggbox fitting a small neighbourhood is an eggbox fitting the corresponding tangent plane.

Thus, the above equations permit to calculate the metric

$$I(x,y) = \begin{bmatrix} \langle \phi_x(x,y), \phi_x(x,y) \rangle & \langle \phi_x(x,y), \phi_y(x,y) \rangle \\ \langle \phi_y(x,y), \phi_x(x,y) \rangle & \langle \phi_y(x,y), \phi_y(x,y) \rangle \end{bmatrix}$$

of $\mathscr{S}$ at M in the parametrization ϕ in terms of the fitting $S^0(M)$ of the tangent plane of $\mathscr{S}$ at M. First, note that, due to periodicity, $U^0(M)$ and $V^0(M)$ are both constant sequences of unitary vectors:

$$\forall n \in \mathbb{Z}, \quad u_n^0(M) = u_o(M), \quad v_n^0(M) = v_o(M).$$

Therefore, up to a rigid body transformation, $(U^0(M), V^0(M))$ are parametrized with one degree of freedom assigned to the interior angle $\theta(x, y)$ of any pyramid converging toward M when r goes to 0. That is to say

$$\cos\theta(x, y) = \langle u_o(M), v_o(M) \rangle .$$

At this stage, it becomes apparent that $I(x, y)$ is a function of $\theta(x, y)$: $I(x, y) =$

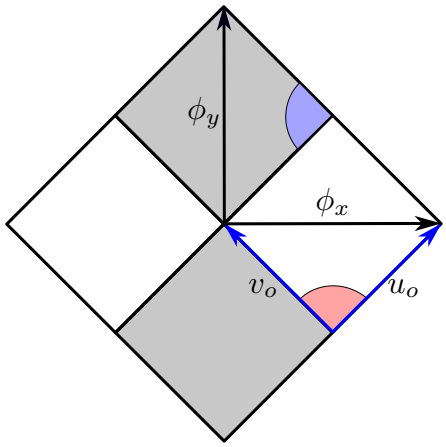

Figure 10. An illustration of the configuration S^0. Only pyramids bases are drawn. The greyed ones correspond to inverted pyramids. Dependency on M was dropped to simplify notations.

$I(\theta(x, y))$. Finally, recalling the definition of θ and θ^* (Figure 10), it is immediate to check that the metric reads

$$I(\theta) = \begin{bmatrix} 4\sin^2(\theta/2) & 0 \\ 0 & 4\sin^2(\theta^*/2) \end{bmatrix}.$$

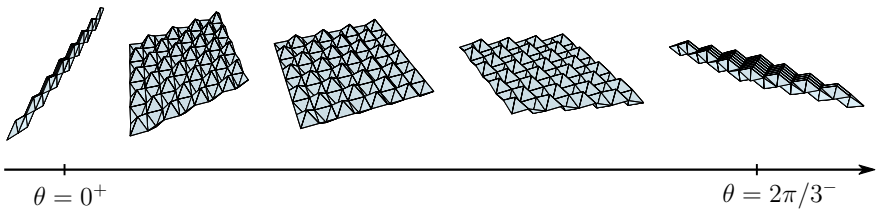

Figure 11. Flat-folding of the eggbox.

As $\theta(x, y)$ changes, the state of the eggbox fitting $\mathscr{S}$, or its tangent plane more precisely, in the vicinity of M changes. For $\theta(x, y) = \pi/2$, all pyramids are in their reference state. For $\theta(x, y) = 0$, the eggbox attached to M is flat-folded in the y direction whereas for $\theta(x, y) = 2\pi/3$, it is flat-folded in the x direction. Figure 11 illustrates this kinematics and shows that the corresponding in-plane Poisson's ratio is positive, that is when one direction is stretched, the transverse cross-section shrinks.

More accurately, when a length ℓ_2 in the y direction deforms by an amount $\varepsilon_2 = \mathrm{d}\ell_2/\ell_2$, a length ℓ_1 in the x direction deforms by an amount $\varepsilon_1 = \mathrm{d}\ell_1/\ell_1$. The Poisson's ratio is then defined as

$$\nu \equiv -\frac{\varepsilon_1}{\varepsilon_2}.$$

In the present case, calculating the in-plane Poisson's ratio is a matter of differentiating $\sin(\theta/2)$ with respect to $\sin(\theta^*/2)$. Elementary considerations entail

$$\nu = -\frac{\sin(\theta^*/2)}{\sin(\theta/2)} \frac{\mathrm{d}\sin(\theta/2)}{\mathrm{d}\sin(\theta^*/2)} = \frac{\tan^2(\theta^*/2)}{\tan^2(\theta/2)} \tag{3}$$

which is positive as expected. Therein, recall that θ can be seen as a function of θ^* owing to Equation (1).

3.4. Local compatibility conditions: on the curvatures

In the same manner, second derivatives of the parametrization ϕ are limits of second rank finite differences based on equivalent vertices. In order to write these, we introduce the finite difference operator Δ_x which acts on a sequence $(M_{i,j})$ to yield the sequence $(\Delta_x M_{i,j})$ satisfying

$$\Delta_x M_{i,j} = M_{i+1,j} - M_{i,j}.$$

Operator Δ_y is similarly defined with respect to the second index. Also, let Δ_{xx} and Δ_{yy} be Δ_x and Δ_y iterated twice, respectively, and Δ_{xy} be the composition of Δ_x and Δ_y. Therefore, the statement that finite differences of rank 2 must converge to their continuous counterparts reads

$$\begin{aligned}
\frac{\Delta_{xx} r M_{i,j}(U^r(M), V^r(M))}{r^2} &\xrightarrow[r\to 0]{} \phi_{xx}(x,y),\\
\frac{\Delta_{yy} r M_{i,j}(U^r(M), V^r(M))}{r^2} &\xrightarrow[r\to 0]{} \phi_{yy}(x,y),\\
\frac{\Delta_{xy} r M_{i,j}(U^r(M), V^r(M))}{r^2} &\xrightarrow[r\to 0]{} \phi_{xy}(x,y).
\end{aligned}$$

It is useful to introduce the first order corrections $\delta M_{i,j}$ to the set of vertices $M_{i,j}(U^0(M), V^0(M))$. These satisfy

$$M_{i,j}(U^r(M), V^r(M)) = M_{i,j}(U^0(M), V^0(M)) + r\delta M_{i,j} + o(r).$$

Accordingly, the above limits simplify into

$$\begin{aligned}
\phi_{xx}(x,y) &= \Delta_{xx}\delta M_{i,j} = \delta M_{i+2,j} - 2\delta M_{i+1,j} + \delta M_{i,j},\\
\phi_{yy}(x,y) &= \Delta_{yy}\delta M_{i,j} = \delta M_{i,j+2} - 2\delta M_{i,j+1} + \delta M_{i,j},\\
\phi_{xy}(x,y) &= \Delta_{xy}\delta M_{i,j} = \delta M_{i+1,j+1} + \delta M_{i,j} - \delta M_{i+1,j} - \delta M_{i,j+1}.
\end{aligned} \tag{4}$$

Therein, we employed the fact that $\Delta_{xx} M_{i,j}(U^0(M), V^0(M))$ vanishes since $S^0(M)$ is periodic.

Inspecting the above equalities, observe that the left hand side is (i,j)-independent so that the first order corrections $\delta M_{i,j}$ are necessarily quadratic in i and in j. It follows then that the first order corrections $\delta U = (\delta u_n)$ and $\delta V = (\delta v_n)$ to the sequences $U^0(M)$ and $V^0(M)$ are *linear* in n. Thus, the first order corrections to the state $S^0(M)$ are completely parametrized with (Figure 12):

1. the correction $\delta\theta$ to the angle $\theta(x,y)$ separating $u_o(M)$ and $v_o(M)$;
2. the vector δu correcting the $u_n^0(M)$ for $n \in \mathbb{Z}$ by increments of $n\delta u$;
3. the vector δv correcting the $v_n^0(M)$ for $n \in \mathbb{Z}$ by increments of $(1-n)\delta v$.

Note that since vectors $u_n^r(M)$ and $v_n^r(M)$ are all unitary, δu and δv are normal to $u_o(M)$ and $v_o(M)$ respectively so that each of them has 2 degrees of freedom instead of 3. Therefore, only 5 degrees of freedom control the first order corrections to the state $S^0(M)$.

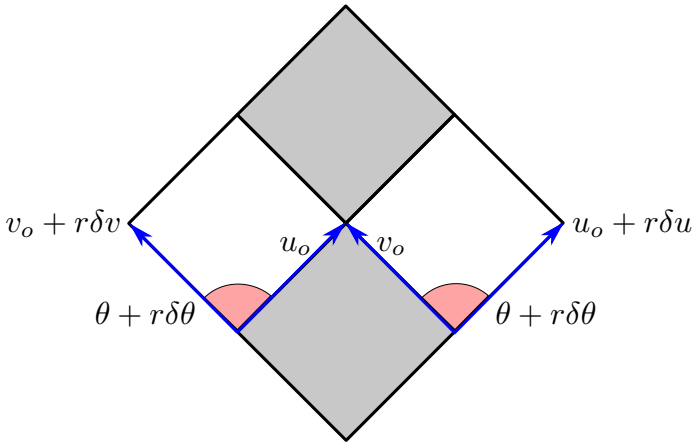

Figure 12. An illustration of the degrees of freedom to first order in r.

In light of the above discussion, $M_{i,j}(U, V)$ being a smooth function of the sequences U and V, the corrections $\delta M_{i,j}$ can be written as linear combinations of the corrections δu_n and δv_n and then as linear combinations of the newly introduced degrees of freedom. Equation (4) can thus be recast into

$$\begin{bmatrix} \phi_{xx}(x,y) \\ \phi_{yy}(x,y) \\ \phi_{xy}(x,y) \end{bmatrix} = \alpha(M) \begin{bmatrix} \delta\theta \\ \delta u \\ \delta v \end{bmatrix},$$

where $\alpha(M)$ is some matrix. In conclusion, after fitting the tangent plane of $\mathscr{S}$ at M with $S^0(M)$, there are a priori 5 degrees of freedom that can be tuned to correct $S^0(M)$ and transform it into a quadratic surface giving the eggbox attached to M the same curvatures as $\mathscr{S}$ at M.

Straightaway however, one remarks that by changing $\theta(x, y)$ the state $S^0(M)$ transforms into another periodic state where all second derivatives are equally vanishing. Accordingly, the first column of matrix $\alpha(M)$ is null and, as far as curvatures are concerned, correcting $\theta(x, y)$ has no impact and we are at liberty to assume that $\delta\theta = 0$. Hence, there exists a matrix $\beta(M)$ such that

$$\begin{bmatrix} \phi_{xx}(x,y) \\ \phi_{yy}(x,y) \\ \phi_{xy}(x,y) \end{bmatrix} = \beta(M) \begin{bmatrix} \delta u \\ \delta v \end{bmatrix}.$$

Therefore, by the rank-nullity theorem, the second derivatives of ϕ need to satisfy $9-4=5$ linear compatibility relations in order to belong to the image space of β. It turns out that 4 out of these 5 relations involve tangential components, i.e., the Christoffel symbols, exclusively and can be obtained by differentiating the metric. These 4 relations provide no additional information. We refer to Appendix A for a definition of the Christoffel symbols and to Appendix B for the list of these 4 relations. As for the 5^{th} compatibility relation, it regards normal components and yields the out-of-plane Poisson's ratio.

In this respect, in a similar manner to how the in-plane Poisson's ratio was defined as the ratio of the strain in the x direction to that in the y direction, we define the out-of-plane Poisson's ratio as the ratio of curvature in the x direction, κ_1, to that in the y direction, κ_2:

$$\nu_{\text{out}} \equiv -\frac{\kappa_1}{\kappa_2}.$$

Therein, the curvatures in the x and y directions are given by

$$\kappa_1 = E/\left\|\phi_x\right\|^2 \quad \text{and} \quad \kappa_2 = G/\left\|\phi_y\right\|^2,$$

where E and G are the diagonal components of the second fundamental form of $\mathscr{S}$ in the parametrization ϕ:

$$II = \begin{bmatrix} E & F \\ F & G \end{bmatrix} \equiv \begin{bmatrix} \langle \phi_{xx}, N\rangle & \langle \phi_{xy}, N\rangle \\ \langle \phi_{xy}, N\rangle & \langle \phi_{yy}, N\rangle \end{bmatrix}.$$

Above, N designates the unitary positively oriented normal vector to $\mathscr{S}$.

Elementary yet lengthy calculations entail then the equality between the in-plane and out-of-plane Poisson's ratios:

$$\nu_{\text{out}} = -\frac{\tan^2(\theta^*/2)}{\tan^2(\theta/2)} = -\nu.$$

The complete analytical proof is detailed in Appendix B.

Surprisingly, the exact same equality (up to a global sign) holds for the well-known Miura-ori tessellation (Schenk and Guest, 2013; Wei et al., 2013). As a matter of fact, Seffen (2012), building on the work of Norman (2009), considered the eggbox as a doubly corrugated shell and observed how it bends into synclastic forms characteristic of auxetic materials even though

the eggbox has a positive in-plane Poisson's ratio. Seffen (2012) also noted that the Miura-ori tessellation has a contradictory behaviour dual to that of the eggbox: it is auxetic but bends into anticlastic shapes. Later, Schenk and Guest (2013) and Wei et al. (2013) proved numerically and analytically, respectively, the above relation for the Miura-ori tessellation. Here, we derive the so-far lacking result for the eggbox pattern and conclude that: the in-plane and out-of-plane Poisson's ratios of the eggbox are equal and opposite to one another, and are equal and opposite to those of the Miura-ori tessellation.

3.5. Conclusion: a continuous formulation of the fitting problem

Given the notations

$$c \equiv \cos(\theta/2), \quad s \equiv \sin(\theta/2), \quad c^* \equiv \cos(\theta^*/2), \quad s^* \equiv \sin(\theta^*/2),$$

the foregoing considerations allow to state the following conclusion.

Let $\mathscr{S}$ be a smooth surface that can be fitted asymptotically by an eggbox. Then, there exist a parametrization ϕ of $\mathscr{S}$ and two functions θ and θ^* satisfying

$$\theta \in]0, 2\pi/3[, \quad \theta^* \in]0, 2\pi/3[, \quad 2cc^* = 1, \tag{5}$$

such that the metric and the second fundamental form of $\mathscr{S}$ with respect to ϕ respectively read

$$I = \begin{bmatrix} 4s^2 & 0 \\ 0 & 4s^{*2} \end{bmatrix} \quad \text{and} \quad II = \begin{bmatrix} E & F \\ F & G \end{bmatrix}$$

with

$$E = \frac{c^2}{c^{*2}} G. \tag{6}$$

We insist on the fact that the above conditions are necessary for the existence of an eggbox fitting. So far we were unable to find a counterexample to the converse. This suggests that these conditions are also sufficient. The latter statement has yet to be proven.

Alternatively, the fundamental theorem of surface theory dictates that finding ϕ is equivalent to finding a set of functions $\{\theta, \theta^*, E, F, G\}$ solution to the Gauss equation

$$\frac{EG - F^2}{16 s^2 s^{*2}} = -\frac{1}{8ss^*} \left[\left(\frac{(s^{*2})_x}{ss^*} \right)_x + \left(\frac{(s^2)_y}{ss^*} \right)_y \right], \tag{7}$$

and to the Codazzi-Mainardi equations

$$E_y - F_x = \frac{(s^2)_y}{2s^2}E + \left(\frac{(s^{*2})_x}{2s^{*2}} - \frac{(s^2)_x}{2s^2}\right)F + \frac{(s^2)_y}{2s^{*2}}G,$$
$$F_y - G_x = -\frac{(s^{*2})_x}{2s^2}E + \left(\frac{(s^{*2})_y}{2s^{*2}} - \frac{(s^2)_y}{2s^2}\right)F - \frac{(s^{*2})_x}{2s^{*2}}G,$$

while satisfying (5) and (6).

Note that the Gauss equation yields the Gaussian curvature in terms of the metric and its derivatives and that the Codazzi-Mainardi equations involve the Christoffel symbols which can be easily calculated given that the metric is a diagonal matrix in the considered parametrization (see Appendix A).

It is also noteworthy that the equality between the in-plane and out-of-plane Poisson's ratios implies a seemingly stronger, vectorial, equality between the second derivatives ϕ_{xx} and ϕ_{yy} which can be cast into the wave equation

$$\phi_{xx}/c^2 - \phi_{yy}/c^{*2} = 0.$$

A short proof is presented in Appendix A. This equation illustrates in a remarkable fashion how the diagonals of the eggbox (Figure 7) propagate genuinely like waves at least to leading order in r.

Finally, the leading order asymptotic method at hand is not limited to the study of the eggbox and generalizes immediately to the study of other pin-jointed trusses and origami tessellations as long as they are periodic. In fact, periodicity is the only feature of the eggbox involved in characterizing the metric and curvatures as asymptotic counterparts to first and second rank finite differences. The shape of the ensuing metric and possible relations between curvatures will of course depend on the particularity of each truss, nonetheless the general results on first and second rank finite differences can be applied to arbitrary periodic trusses.

4. Examples of fitted surfaces

Here, some solutions $\mathscr{S}$ to the fitting problem formulated in the foregoing section are constructed, fitted and analysed to illustrate both the deformation modes of the eggbox and the pertinence of the suggested continuous approach. In particular, we completely characterize axisymmetric fittings and explore a degenerate limit where the truss is flat-folded which turns out to be suitable for fitting ruled surfaces.

4.1. Uniform fittings

As a first example, we consider smooth surfaces which can be fitted uniformly. By that we mean that the pyramids of the fitting eggbox are in the same configuration everywhere up to a rigid body motion. In other words, the matrices of the first and second fundamental forms of these surfaces, in the parametrization ϕ, are (x, y)-independent. Note that the Gauss equation, Equation (7), implies in particular that these surfaces are necessarily developable.

Let $\mathscr{S}$ be such a surface. Then its parametrization ϕ is solution to the wave equation

$$\phi_{xx}/c^2 - \phi_{yy}/c^{*2} = 0,$$

where c and c^* are now constants. Standard analysis entails that $\mathscr{S}$ is a sum of two curves, i.e., a surface of translation,

$$\phi(x, y) = \xi(x/c^* + y/c) + \eta(x/c^* - y/c).$$

One of these two curves, say the one parametrized with ξ, is necessarily a straight line since the Gaussian curvature is identically null:

$$\phi(x, y) = (x/c^* + y/c)\xi + \eta(x/c^* - y/c).$$

Therein, ξ now designates a constant vector. The surface $\mathscr{S}$ is then the sum of a curve and a straight line, i.e., a cylinder.

When η describes a straight line as well, $\mathscr{S}$ corresponds to one of the plane states of the flat-folding motion of Figure 11. From there, the above formula says that, in any further deformation keeping θ constant, the level sets of $x/c^* - y/c$ have to remain straight lines collinear to ξ whereas the level sets of $x/c^* + y/c$ can be wrapped around ξ to generate a cylinder of an arbitrary cross section. For $\theta = \pi/2$, we recover the trivial result that it is possible to fit any cylinder by laying the fibres $x - y = \text{cste}$ in the direction of the axis and wrapping the orthogonal fibres $x + y = \text{cste}$ around the axis to fit the cross section.

So far, we have only used the fact that I is constant and concluded that $\mathscr{S}$ is necessarily a cylinder. When, in addition, II is constant, the curvature of the cross section becomes constant and $\mathscr{S}$ a circular cylinder. Figure 13 illustrates the fact and depicts a flat-folding motion over cylindrical states where θ changes but the fitted circular cylinder remains the same. Last, note that the pyramidal truss was able to fit developable surfaces other than cylinders with a constant θ. In contrast, in order to fit non-cylindrical developable surfaces with an eggbox, θ has to vary across pyramids.

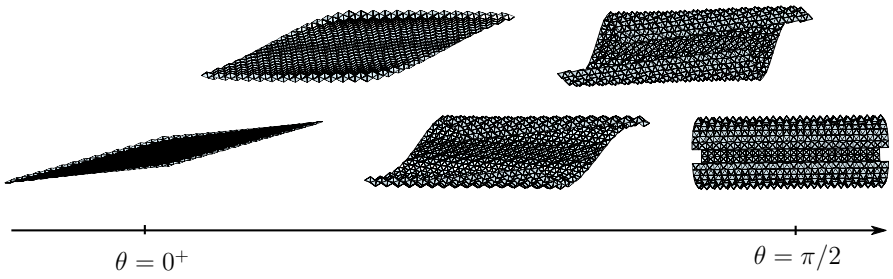

Figure 13. Flat-folding of the eggbox through cylindrical states of the same radius.

4.2. Plane axisymmetric fittings

The plane modes of the eggbox are characterized by $II = 0$. The only non-trivial equation is Gauss's (7)

$$0 = \left(\frac{(s^{*2})_x}{ss^*}\right)_x + \left(\frac{(s^2)_y}{ss^*}\right)_y$$

which describes how the metric, or θ, varies within the fitted plane. For axisymmetric configurations, θ is a function of one variable, say y, and we are able to go one step further by affirming that

$$\frac{(s^2)_y}{ss^*} = \gamma,$$

where γ is an integration constant. When γ is non-null, it is always possible to invert and scale the y-axis so that γ becomes positive and equal to 1. If so, s_y is of a constant positive sign and θ is strictly increasing from 0 to $2\pi/3$ and entirely determined by

$$\int_0^{s^2} \frac{\mathrm{d}s^2}{ss^*} = y.$$

Recall that both s and s^* are functions of θ so that s^* can be written as a function of s. Therein, we have assumed that the eggbox is flat-folded at $y = 0$ ($\theta(x, 0) = 0$). At the other end $y = y_{\max}$, the eggbox is equally flat-folded but in the orthogonal direction ($\theta(x, y_{\max}) = 2\pi/3$). Regarding this, we have

$$\int_0^{3/4} \frac{\mathrm{d}s^2}{ss^*} = y_{\max}.$$

Finally, if γ is null, s is a constant and we recover the plane flat-folding mode.

In light of the above discussion, it appears that the eggbox admits one non-uniform plane axisymmetric mode which is unique up to a plane symmetry interchanging the x and y axes combined with a homothety of an arbitrary scaling factor (Figure 14).

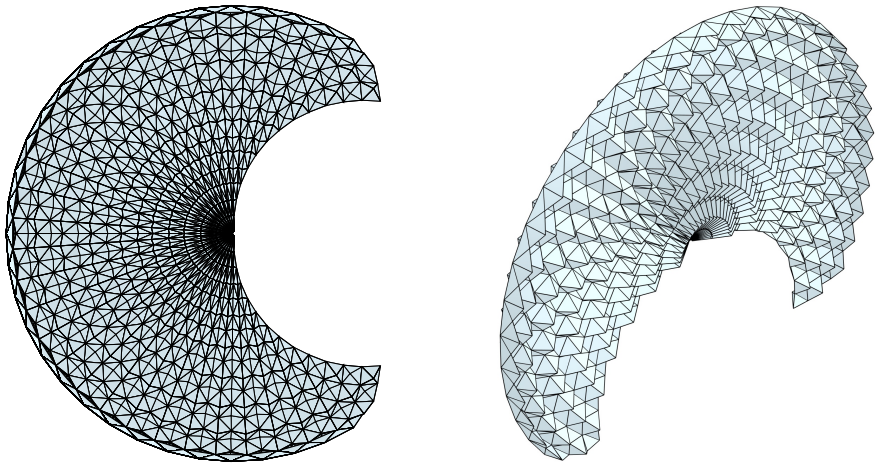

Figure 14. The unique plane axisymmetric mode of the eggbox.

4.3. General axisymmetric fittings

Here, we argue that there exists only one one-parameter family of axisymmetric fittings unique up to the symmetry interchanging x and y combined with a homothety of an arbitrary scaling factor. The plane fittings obtained so far can be derived as limiting cases and are excluded in the following.

Consider a surface $\mathscr{S}$ fitted axisymmetrically with an eggbox. Then, I and II are functions of one variable, say y. Thus, solving the fitting problem amounts to solving an autonomous system of differential equations implying that $\mathscr{S}$ is completely determined by the initial values of θ, θ_y, E and F. Hereafter, we argue that F is constantly vanishing and that there exists a point y_M at which θ_y vanishes. Seeking uniqueness up to a homothety, it is legitimate to assume that E equals 1 at y_M. Finally, we can conclude that $\mathscr{S}$ is entirely determined by the value taken by θ at y_M.

It is clear that x parametrizes a series of rotations around some fixed axis leaving the eggbox invariant. Hence, the derivative of the normal vector with

respect to x, N_x, is collinear to ϕ_x. It follows immediately that

$$F = \langle \phi_{xy}, N \rangle = \langle \phi_y, N \rangle_x - \langle \phi_y, N_x \rangle = 0$$

since ϕ_y is orthogonal to both N and ϕ_x. It is worth noting that F being null, the Gaussian curvature is proportional to EG which is positive by the negativity of the out-of-plane Poisson's ratio.

Thanks to the previous preliminary, one of the two Codazzi-Mainardi equations becomes trivial whereas the other one simplifies into

$$E_y = \frac{(s^2)_y}{2s^2} E + \frac{(s^2)_y}{2s^{*2}} G.$$

The relationship between E and G together with the chain rule allows us to obtain

$$\frac{E_y}{E} = \frac{(s^2)_y}{2s^2} + \frac{(s^2)_y}{2s^{*2}} \frac{G}{E} = \frac{(s^2)_y}{2s^2} - \frac{(s^2)_y}{2s^{*2}} \frac{\mathrm{d}s^{*2}}{\mathrm{d}s^2} = \frac{(s^2)_y}{2s^2} - \frac{(s^{*2})_y}{2s^{*2}},$$

which easily integrates into

$$\frac{E}{E_o} = \frac{s/s_o}{s^*/s_o^*},$$

where E_o, s_o and s_o^* are some initial values of the concerned quantities.

Now, call R the radius of the cross section of $\mathscr{S}$ orthogonal to its axis. We will prove that R is maximum at some point $y = y_M$. In fact, the uniform circular motion described with the variable x means that the velocity $\|\phi_x\| = 2s$ is proportional[1] to the radius R of the motion. Since s is bounded, R is bounded as well. Summarizing what we know so far, the radius of the cross section R is a positive bounded function of y and is concave by the positivity of the Gaussian curvature leaving only two possible scenarii. The first one is that R reaches a maximum, which is what we are after. The other one is that R grows indefinitely approaching an asymptotic value. Near the asymptote, R is virtually constant, $\mathscr{S}$ resembles a circular cylinder and the Gaussian curvature as well as E and G are approximately null. However, when E is zero, the integrated Codazzi-Mainardi equation yields $s/s^* = 0$. Thus, asymptotically s is null and so is R by proportionality. This is absurd

[1]Intuitively, R/s estimates the number of pyramids constituting a cross section. This number has to be conserved from one section to the other.

unless R is constantly null. In any case, we conclude that R is maximum at some point $y = y_M$.

When y_M is an interior point of the domain of definition of R, it is assured that the derivative of R is null at y_M. Otherwise, y_M is at the extremity of the domain of definition and the fitting cannot be extended beyond that point. In such case, at y_M, either $\theta = 0$ or $\theta = 2\pi/3$. Assuming $\theta = 0$ implies that $s = 0$ and $R = 0$. Then, 0 is the maximum of R which is consequently constantly null, the eggbox is flat-folded and $\mathscr{S}$ is degenerate. The other possibility is that θ reaches $2\pi/3$ at y_M. Hence, s^* is null at y_M and the integrated Codazzi-Mainardi equation entails that E becomes unbounded unless E_o was null. As a consequence, E is constantly null and so is G and the eggbox is in the previously considered plane axisymmetric configuration. This being excluded concludes our proof that y_M is an interior point and that R, as well as s and θ, have zero derivatives at y_M where they reach their respective maxima.

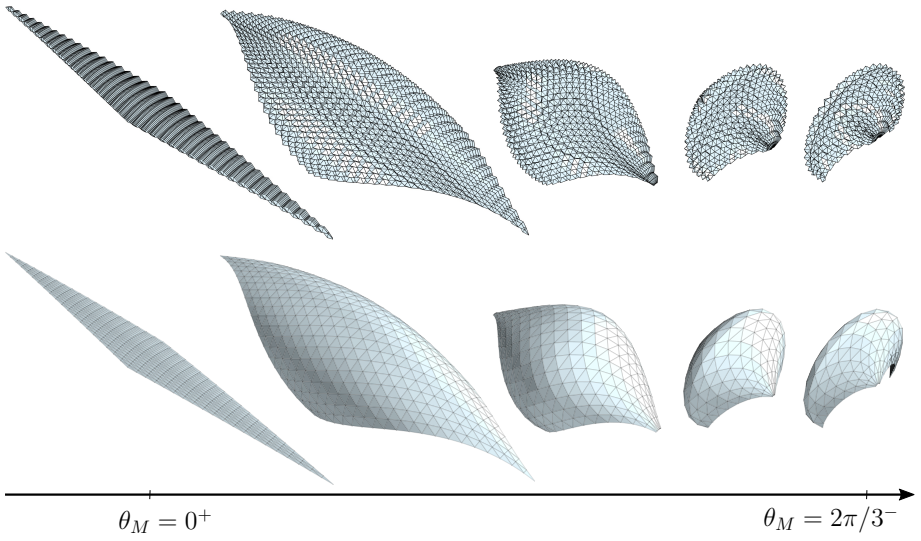

Figure 15. The unique one-parameter family of axisymmetric fittings. The depicted configurations all have the same number of pyramids and the same maximum radius R_M. The maximum interior angle θ_M is reached at R_M and is varied from 0^+ to $2\pi/3^-$. The first row depicts the eggbox entirely whereas in the second one, only a set of equivalent vertices is plotted.

Figure 15 depicts the unique one-parameter family of axisymmetric fittings

parametrized by the interior angle θ_M of the pyramids located at $y = y_M$. They all have positive Gaussian curvature as noted earlier. When the radius R_M of $\mathscr{S}$ is scaled to infinity, we recover the plane flat-folding mode, and when θ_M approaches $2\pi/3$, we recover the plane axisymmetric mode.

4.4. Ruled surfaces

The fittings encountered until now were either of zero or of positive Gaussian curvature. The eggbox is also capable of fitting some saddle-shaped surfaces. An example is depicted in Figure 16. Here, we prove that if a smooth surface $\mathscr{S}$ is fitted by an almost flat-folded eggbox, then $\mathscr{S}$ is necessarily a ruled surface. Ruled surfaces include all developable surfaces and a rich family of negatively curved surfaces.

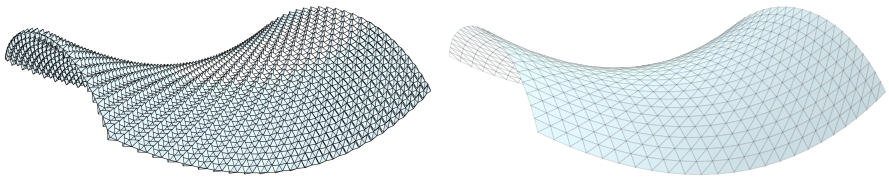

Figure 16. A saddle-shaped fitted surface. Here, θ is far from 0.

We consider a smooth surface $\mathscr{S}$ fitted with an eggbox in which θ is uniformly close to 0. The surface $\mathscr{S}$ being smooth, its curvatures in the x and y directions, κ_1 and κ_2, have to remain finite. Now, when θ approaches 0, the Poisson's ratio ν tends to infinity (Equation (3)). Given that $\kappa_1/\kappa_2 = \nu$, we conclude that κ_2 is arbitrarily small and that $\kappa_1 = \nu\kappa_2$ is indeterminate. Therefore, asymptotically, the eggbox straightens in the y direction. In the limit, κ_2 is rigorously null and the level sets of x are straight lines.

Formally speaking, it is convenient to introduce a small parameter ϵ quantifying the distance between θ and 0. We write

$$\theta = \epsilon\theta_o + o(\epsilon),$$

where θ_o is the first order term of the expansion of θ in the vicinity of 0. Then, we perform the change of variables $X = \epsilon x$, $Y = y$. This is motivated by the fact that when θ is of order ϵ, crossing a finite distance in the x direction requires taking large values of x of order $1/\epsilon$. In the new coordinates, we have

$$I = \begin{bmatrix} 4s^2/\epsilon^2 & 0 \\ 0 & 4s^{*2} \end{bmatrix} \quad \text{and} \quad I\!I = \begin{bmatrix} E/\epsilon^2 & F/\epsilon \\ F/\epsilon & G \end{bmatrix}.$$

Accordingly, a smooth limit surface $\mathscr{S}$ exists only under the conditions

$$E = \epsilon^2 E_o + o(\epsilon^2) \quad \text{and} \quad F = \epsilon F_o + o(\epsilon).$$

Hence, $G = o(\epsilon)$ because $E/G = c^2/c^{*2} = 4 + o(\epsilon)$.

Finally, the fitting problem, to the leading order in ϵ, amounts to finding a smooth parametrization ϕ in which the first and the second fundamental forms of $\mathscr{S}$ read respectively

$$I = \begin{bmatrix} \theta_o^2 & 0 \\ 0 & 3 \end{bmatrix} \quad \text{and} \quad II = \begin{bmatrix} E_o & F_o \\ F_o & 0 \end{bmatrix}.$$

A direct consequence is that ϕ_{YY} is orthogonal to ϕ_X, to ϕ_Y and to N. Hence, ϕ_{YY} is constantly null[2] and $\mathscr{S}$ is a ruled surface.

We have already seen the precursor of these surfaces when studying axisymmetric fittings. As a matter of fact, in the vicinity of the singularities of these fittings (on Figure 15, where the pyramids collapse and θ is null), $\mathscr{S}$ resembles a cone. By scaling that region properly, it is possible to obtain an asymptotic fitting of a cone. Figure 17 portrays the limit process.

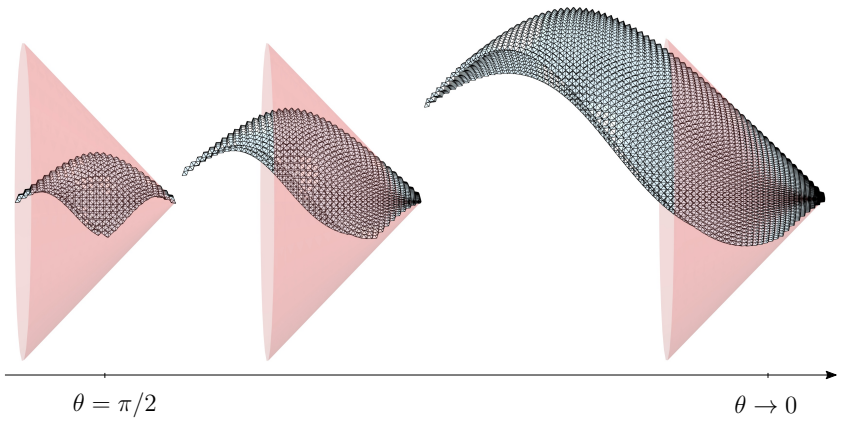

Figure 17. Fitting a cone with an eggbox. The angle θ refers to the interior angle of the pyramids located at a cross section at a fixed finite distance from the cone vertex. The number of pyramids used each time grows accordingly.

[2]Otherwise, substitute $b = 3$ and $G = 0$ in Equation (A.1) and recover $\phi_{YY} = 0$.

5. Conclusion

In the spirit of homogenization theory, it is advantageous to have a continuous model describing the mechanical behaviour of a discrete structure especially when it is composed of a large number of constitutive elements. Here, a two-scale asymptotic method is deployed to obtain continuous models for the kinematics of periodic pin-jointed trusses, i.e., periodic assemblies of rigid bars and pivots. The compatible deformation modes are found to be solutions of a system of partial differential equations. In other words, our conclusions state that the smooth surfaces that can be fitted by a given periodic truss have metric and curvature fields that, in a certain parametrization, satisfy a known set of partial differential equations. These equations are derived for a fairly generic example, the eggbox, using analytical techniques easily transposable to the study of other structures such as Origami and Kirigami tessellations.

The present asymptotic method has the merit of avoiding to deal with a formidable number of discrete degrees of freedom. In fact, it only requires a knowledge of the quadratic states of the truss and these can be obtained by inspecting a few unit-cells. Quadratic states contain information on both metric and curvatures which are enough to locally characterize any fitted smooth surface. In order to obtain a global characterization, standard tools from differential geometry of surfaces, the Gauss-Codazzi-Mainardi equations in particular, are exploited.

It is worth noting that the presented method presumes neither infinitesimal displacements nor infinitesimal strains. As a matter of fact, all of the exemplified fittings were predicted correctly while they exhibit large deformations at the level of unit-cells as well as on the continuous level. Nonetheless, microscopic buckling modes involving a finite number of unit-cells per wavelength are precluded (Figure 18). To take them into account, non-minimal unit-cells should be considered.

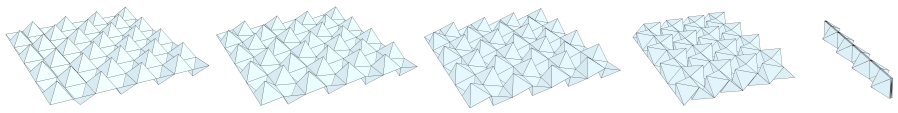

Figure 18. A microscopic buckling mode of the eggbox.

One can check numerically the convergence of the used asymptotics (Fig-

ure 19). Then, at convergence, the kinematics of the eggbox is the one described in this paper to leading order. Nonetheless, characterizing surfaces which can be fitted before convergence may be of great interest. This is true when the characteristic length r is small but not infinitely small compared to the radius of curvature of the surface to be fitted or, conversely, when the fitting does not contain a large enough number of unit-cells. In these cases, the use of leading order asymptotics is not well justified.

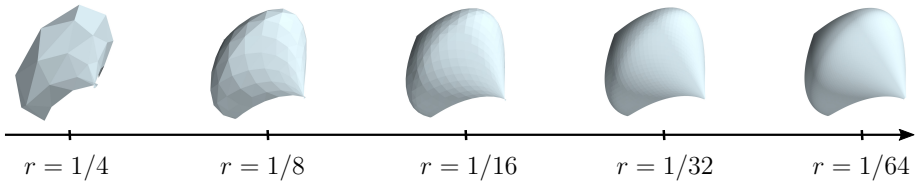

Figure 19. An illustration of the convergence of an axisymmetric fitting as $r \to 0$. The maximum radius and maximum interior angle are kept constant while r decreases.

On a similar note, we have found that the metric of a fitted surface is a function of the possible periodic states of the eggbox. In contrast, when a truss has only one periodic state and no (plane) periodic deformation mode, the metric of any fitted surface will be one-valued implying that the fitted surface has zero Gaussian curvature and is developable. We have proven then the corollary: when a truss has no periodic deformation mode, it can only fit developable surfaces to leading order in r. One example is the pyramidal truss of Section 2. Another example is the Ron-Resch origami tessellation. This seems to contradict our empirical experience when manipulating these structures since they both can deform into sphere-like and saddle-shaped surfaces (see, e.g., Figure 1). In light of the above discussion, we argue that this is possible because usually the manipulated structures contain only a small limited number of unit-cells or that the constructed surfaces have radii of curvature of the same order of magnitude as the unit-cell size. A similar observation based on discrete considerations was made by Tachi (2015).

Asymptotically expanding beyond the leading order will make appear a direct dependence on the internal length r and should improve the predictions of the method in "non-converged" situations. Exploring this possibility for

the eggbox and other trusses should help better understand which surfaces can or cannot be fitted and why.

Acknowledgement

This work has benefited from a French government grant managed by ANR within the frame of the national program Investments for the Future ANR-11-LABX-022-01. The authors would also like to thank L. Hauswirth (LAMA, University Paris-Est) for helpful discussions.

References

Belcastro, S.M., Hull, T.C., 2002. Modelling the folding of paper into three dimensions using affine transformations. Linear Algebra and its Applications 348, 273–282.

Blinn, J., 1988. The world's largest easter egg and what came out of it. IEEE Computer Graphics and Applications 8, 16–23.

Ciarlet, P.G., 2006. An introduction to differential geometry with applications to elasticity. Springer, Dordrecht.

Dell'Isola, F., Giorgio, I., Pawlikowski, M., Rizzi, N.L., 2016. Large deformations of planar extensible beams and pantographic lattices: heuristic homogenization, experimental and numerical examples of equilibrium. Proceedings of the Royal Society of London A: Mathematical, Physical and Engineering Sciences 472, 20150790.

Demaine, E.D., Demaine, M.L., Hart, V., Price, G.N., Tachi, T., 2011. (Non)Existence of pleated folds: How paper folds between creases. Graphs and Combinatorics 27, 377–397.

Dudte, L.H., Vouga, E., Tachi, T., Mahadevan, L., 2016. Programming curvature using origami tessellations. Nature Materials 15, 583–588.

Ghys, E., 2011. Sur la coupe des vêtements: Variation autour d'un thème de Tchebychev. L'Enseignement Mathématique 57, 165–208.

Hochfeld, H., 1959. Process and Machine for Pleating pliable materials. US2901951 .

Korte, A.P., Starostin, E.L., Van Der Heijden, G.H.M., 2010. Triangular buckling patterns of twisted inextensible strips. Proceedings of the Royal Society of London A , 285–303.

Lang, R.J., 2003. Origami Design Secrets: Mathematical Methods for an Ancient Art. CRC Press.

Lebée, A., 2015. From folds to structures, a review. International Journal of Space Structures 30, 55–74.

Lechenault, F., Thiria, B., Adda-Bedia, M., 2014. Mechanical response of a creased sheet. Physical Review Letters 112, 244301.

Lv, C., Krishnaraju, D., Konjevod, G., Yu, H., Jiang, H., 2014. Origami based Mechanical Metamaterials. Scientific Reports 4.

Masson, Y., Monasse, L., 2016. Existence of global Chebyshev nets on surfaces of absolute Gaussian curvature less than 2π. Journal of Geometry doi:10.1007/s00022-016-0319-1.

Milton, G.W., Cherkaev, A.V., 1995. Which elasticity tensors are realizable? Journal of engineering materials and technology 117, 483–493.

Miura, K., 1985. Method of packaging and deployment of large membranes in space. The institute of Space and Astronautical Science Report 618, 1–9.

Norman, A.D., 2009. Multistable and morphing corrugated shell structures. Ph.D. thesis. University of Cambridge.

Norris, A.N., 2008. Acoustic cloaking theory. Proceedings of the Royal Society of London A: Mathematical, Physical and Engineering Sciences 464, 2411–2434.

Peraza-Hernandez, E.A., Hartl, D.J., Malak Jr, R.J., Lagoudas, D.C., 2014. Origami-inspired active structures: a synthesis and review. Smart Materials and Structures 23, 094001.

Resch, R.D., Christiansen, H., 1970. The design and analysis of kinematic folded-plate systems. Proceedings of IASS Symposium on folded plates and prismatic structures .

Samelson, S.L., Dayawansa, W.P., 2012. On the existence of global Tchebychev nets. Transactions of the American Mathematical Society 347, 651–660.

Schenk, M., Guest, S.D., 2011. Origami folding: A structural engineering approach, in: Wang-Iverson, P. and Lang, R.J. and YIM, M. (Ed.), Proceedings of The Fifth International Meeting of Origami Science Mathematics and Education (5OSME), pp. 291–303.

Schenk, M., Guest, S.D., 2013. Geometry of Miura-folded metamaterials. Proceedings of the National Academy of Sciences 110, 3276–3281.

Seffen, K.A., 2012. Compliant shell mechanisms. Philosophical Transactions of the Royal Society A: Mathematical, Physical and Engineering Sciences 370, 2010–2026.

Seppecher, P., Alibert, J.J., Dell'Isola, F., 2011. Linear elastic trusses leading to continua with exotic mechanical interactions. Journal of Physics: Conference Series 319, 012018.

Silverberg, J.L., Evans, A.A., McLeod, L., Hayward, R.C., Hull, T., Santangelo, C.D., Cohen, I., 2014. Using origami design principles to fold reprogrammable mechanical metamaterials. Science 345, 647–650.

Tachi, T., 2009. Simulation of rigid origami. Proceedings of the 4th International Meeting of Origami Science, Math, and Education (4OSME) , 175–187.

Tachi, T., 2010. Origamizing polyhedral surfaces. IEEE transactions on visualization and computer graphics 16, 298–311.

Tachi, T., 2013. Designing freeform origami tessellations by generalizing Resch's patterns. Journal of mechanical design 135, 111006.

Tachi, T., 2015. Rigid folding of periodic origami tessellations, in: Miura, K., Kawasaki, T., Tachi, T., Uehara, R., Lang, R.J., Wang-Iverson, P. (Eds.), Proceedings of the 6th International Meeting of Origami Science, Math, and Education (6OSME): I. Mathematics, pp. 97–108.

Wei, Z.Y., Guo, Z.V., Dudte, L., Liang, H.Y., Mahadevan, L., 2013. Geometric Mechanics of Periodic Pleated Origami. Physical Review Letters 110, 215501.

You, Z., 2014. Folding structures out of flat materials. Science 345, 623–624.

Zhou, X., Wang, H., You, Z., 2015. Design of three-dimensional origami structures based on a vertex approach. Proceedings of the Royal Society of London A: Mathematical, Physical and Engineering Sciences 471, 20150407.

Appendix A. Christoffel symbols of a diagonal metric

Let $\mathscr{S}$ be a smooth surface of ϕ. Then the family (ϕ_x, ϕ_y, N) is a basis of the space $\mathbb{R}^3$ in which $\mathscr{S}$ is embedded. Hence, the second derivatives ϕ_{xx}, ϕ_{yy} and ϕ_{xy} can be expanded relatively to that basis. For instance, one has

$$\phi_{xx} = \Gamma^1_{11}\phi_x + \Gamma^2_{11}\phi_y + EN$$

where the Γ coefficients are known as Christoffel symbols and E is the first coefficient of the second fundamental form II.

It is known that the Christoffel symbols can be written in terms of the metric I of $\mathscr{S}$ and of its first derivatives. When I is diagonal, i.e., ϕ_x and ϕ_y are orthogonal, these expressions are particularly simple. Here, we calculate Γ^1_{11} as an example. Indeed, one has

$$\Gamma^1_{11} = \frac{\langle \phi_{xx}, \phi_x \rangle}{\langle \phi_x, \phi_x \rangle} = \frac{1}{2}\frac{\langle \phi_x, \phi_x \rangle_x}{\langle \phi_x, \phi_x \rangle}.$$

As for the other Christoffel symbols, denoting

$$I = \begin{bmatrix} a & 0 \\ 0 & b \end{bmatrix},$$

one has

$$\begin{aligned} \phi_{xx} &= \frac{a_x}{2a}\phi_x - \frac{a_y}{2b}\phi_y + EN \\ \phi_{yy} &= -\frac{b_x}{2a}\phi_x + \frac{b_y}{2b}\phi_y + GN \\ \phi_{xy} &= \frac{a_y}{2a}\phi_x + \frac{b_x}{2b}\phi_y + FN. \end{aligned} \tag{A.1}$$

These are sometimes referred to as the frame equations.

Finally, the in-plane and out-of-plane Poisson's ratios being equal and of opposite signs reads

$$\frac{\mathrm{d}\sqrt{a}/\,\mathrm{d}\sqrt{b}}{\sqrt{a}/\sqrt{b}} = -\frac{E/a}{G/b},$$

which, upon simplification, transforms into

$$\frac{\mathrm{d}a}{\mathrm{d}b} = -\frac{E}{G}.$$

It is then remarkable that, due to the first two frame equations together with the chain rule, the above scalar equation translates into the vectorial partial differential equation

$$\phi_{xx}/E - \phi_{yy}/G = 0.$$

Appendix B. Out-of-plane Poisson's ratio

Consider the set of vertices depicted in Figure B.20. Note that vertices O, A, B, C and D are equivalent so that we have

$$\phi_{xx} = \frac{A + C - 2O}{r^2} + o(1) \quad \text{and} \quad \phi_{yy} = \frac{B + D - 2O}{r^2} + o(1).$$

Therein and hereafter dependency over M was dropped to simplify notations.

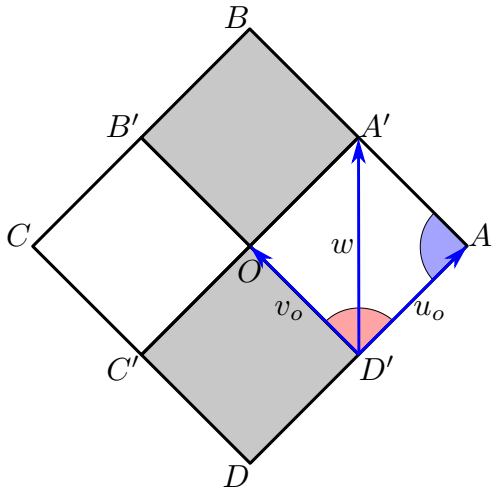

Figure B.20. A set of vertices, depicted prior to perturbation, allowing to estimate the second derivatives of ϕ. Vectors u_o and v_o are unitary and here, along with vector w, they are scaled by a factor r.

These vertices being initially in a periodic state corresponding to S^0, the above relations transform into

$$\phi_{xx} = \delta A + \delta C - 2\delta O \quad \text{and} \quad \phi_{yy} = \delta B + \delta D - 2\delta O,$$

where the δ quantities are corrections to the location of vertices dictated by $\delta\theta$, δu and δv. However, $\delta\theta$ having no impact on second derivatives, it is legitimate to assume that one of the 4 inspected pyramids, say $OC'DD'$, remains in its initial state. Correspondingly,

$$\delta O = \delta D' = \delta D = \delta C' = 0,$$

and

$$\phi_{xx} = \delta A + \delta C \quad \text{and} \quad \phi_{yy} = \delta B.$$

Now let us calculate the following scalar products.

1. The correction δA is orthogonal to u_o so that

$$\langle \phi_{xx}, u_o \rangle = \langle \delta C, u_o \rangle .$$

Also,

$$\langle \phi_{xx}, v_o \rangle = \langle \delta A, v_o \rangle .$$

2. The correction $\delta B - \delta B'$ is orthogonal to $\overrightarrow{B'B}$ which is collinear to u_o by periodicity of the initial state. Hence,

$$\langle \phi_{yy}, u_o \rangle = \langle \delta B, u_o \rangle = \langle \delta B', u_o \rangle .$$

Also,

$$\langle \phi_{yy}, v_o \rangle = \langle \delta B, v_o \rangle = \langle \delta A', v_o \rangle .$$

3. We already know that vector w can be written in terms of u_o and v_o. Furthermore, by symmetry, w is a linear combination of $u_o + v_o$ and $u_o \wedge v_o$. Therefore, there exist two functions a and b satisfying

$$\begin{aligned} w = w(u_o, v_o) &= a(\langle u_o, v_o \rangle)(u_o + v_o) + b(\langle u_o, v_o \rangle) u_o \wedge v_o \\ &= a(\cos\theta)(u_o + v_o) + b(\cos\theta) u_o \wedge v_o. \end{aligned}$$

Thus,

$$\begin{aligned} \langle \delta A', v_o \rangle &= \left\langle \frac{w(u_o + r\delta A, v_o) - w(u_o, v_o)}{r}, v_o \right\rangle + o(1) \\ &= \langle a(\cos\theta)\delta A + a'(\cos\theta) \langle \delta A, v_o \rangle (u_o + v_o), v_o \rangle \\ &= [a(\cos\theta) + a'(\cos\theta)(1 + \cos\theta)] \langle \delta A, v_o \rangle , \end{aligned}$$

with $a' = \mathrm{d}a/\mathrm{d}\cos\theta$. Similarly,

$$\langle \delta B', u_o \rangle = [a(\cos\theta) + a'(\cos\theta)(1 + \cos\theta)] \langle \delta C, u_o \rangle .$$

Recalling the definition of θ^*, it is easy to check that both

$$a(\cos\theta) = \frac{\langle w(u_o, v_o), u_o + v_o\rangle}{\langle u_o + v_o, u_o + v_o\rangle} = \sin^2(\theta^*)$$

and

$$a(\cos\theta) + a'(\cos\theta)(1 + \cos\theta) = \frac{\cos^2(\theta^*/2)}{\cos^2(\theta/2)}$$

hold. Consequently, we have proven the identity

$$\langle \phi_{yy}, u_o + v_o\rangle = \frac{\cos^2(\theta^*/2)}{\cos^2(\theta/2)} \langle \phi_{xx}, u_o + v_o\rangle .$$

Decomposing $u_o + v_o$ into tangential and normal components, we finally derive the compatibility relation

$$\langle \phi_{yy}, N\rangle = \frac{\cos^2(\theta^*/2)}{\cos^2(\theta/2)} \langle \phi_{xx}, N\rangle$$

implying the equality between the in-plane and out-of-plane Poisson's ratios:

$$\nu_{\text{out}} = -\frac{\tan^2(\theta^*/2)}{\tan^2(\theta/2)} = -\nu.$$

The other 4 compatibility relations involving the tangential components can be derived directly from the metric. The first two are obtained by differentiating

$$\langle \phi_x, \phi_y\rangle = 0$$

with respect to x and y and respectively read

$$\begin{aligned} \langle \phi_{xx}, \phi_y\rangle + \langle \phi_x, \phi_{xy}\rangle &= 0, \\ \langle \phi_{xy}, \phi_y\rangle + \langle \phi_x, \phi_{yy}\rangle &= 0. \end{aligned}$$

The second two are obtained by differentiating Equation (1), i.e.,

$$4(1 - \langle \phi_x, \phi_x\rangle /4)(1 - \langle \phi_y, \phi_y\rangle /4) = 1,$$

with respect to x and y and respectively read

$$\begin{aligned} -c^{*2} \langle \phi_{xx}, \phi_x\rangle - c^2 \langle \phi_{xy}, \phi_y\rangle &= 0, \\ -c^{*2} \langle \phi_{xy}, \phi_x\rangle - c^2 \langle \phi_{yy}, \phi_y\rangle &= 0. \end{aligned}$$